K-shell excitation of the water, ammonia, and methane molecules using high-resolution photoabsorption spectroscopy

J. Schirmer and A. B. Trofimov*
Theoretische Chemie, Physikalisch-Chemisches Institut, Universität Heidelberg, 6900 Heidelberg, Federal Republic of Germany

K. J. Randall, J. Feldhaus, and A. M. Bradshaw
Fritz-Haber-Institut der Max-Planck-Gesellschaft, Faradayweg 4-6, 1000 Berlin 33, Federal Republic of Germany

Y. Ma, C. T. Chen, and F. Sette
AT&T Bell Laboratories, 600 Mountain Avenue, Murray Hill, New Jersey 07947
(Received 10 August 1992)

The K-shell excitation spectra of the hydrides water, ammonia, and methane have been measured in photoabsorption experiments using synchrotron radiation in combination with a high-resolution monochromator. For the case of methane, in particular, a wealth of spectral detail is observed which was not accessible in previous studies. The measured excitation energies and relative intensities compare well with values calculated using a complete second-order approximation for the polarization propagator. In order to determine the extent of admixing of valence excitations (i.e., transitions into virtual σ^* orbitals) to the Rydberg manifolds, the X-H bond lengths have been varied in the calculations. In the case of H_2O, the two lowest-energy bands are due to the O $1s$-$4a_1/3s$ and O $1s$-$2b_2/3p$ transitions and have strong valence character; their width indicates that both excitations are dissociative. The NH_3 and ND_3 spectra are also broad which is not only due to possible dissociation but also to unresolved vibrational fine structure (ν_2 mode) and a Jahn-Teller instability. Valence character is concentrated in the lowest excited state in the Rydberg ns manifold, but is distributed more uniformly over the $np(e)$ manifold. The weak dipole-forbidden C $1s$-$3s(a_1)$ transition in CH_4 and CD_4 is accompanied by vibrational structure due to the ν_4 mode, indicating that it derives its intensity from vibronic coupling with the C $1s$-$3p(t_2)$ transition. The structure on the latter band is extremely complicated due to Jahn-Teller coupling and cannot be assigned at present, as is the case for the Rydberg transitions at higher energies. The higher np Rydberg excitations contain considerable valence character.

PACS number(s): 33.20.Rm, 35.20.−i

I. INTRODUCTION

K-shell excitation of the CH_4, NH_3, and H_2O molecules has been studied in the past using both electron-energy-loss spectroscopy (EELS) [1–4] and x-ray absorption spectroscopy [5–9]. Although the spectral resolution obtained with the latter technique has generally been rather modest and could not match that of EELS, recent advances in grazing-incidence monochromator design [10–14] have resulted in a dramatic improvement of resolution with the "optical" approach. This has been shown in a number of high-resolution K-shell excitation spectra of small molecules reported recently (e.g., Refs. [15–19]). In the present paper we describe measurements of the photoabsorption spectrum of gas phase H_2O, NH_3, and CH_4 in the near-K-edge region at a resolution sufficiently high to reveal directly the spectral line shape. To substantiate the assignments we have also calculated excitation energies and oscillator strengths using a polarization propagator method [20].

In the virtual orbital spectrum of these hydrides and other saturated molecules one expects antibonding valence-type (σ^*) orbitals which are the counterparts of the occupied bonding X-H orbitals. An important question is to what extent this antibonding valence character appears in the excitation spectrum. In most of the earlier K-shell studies on the hydrides, the features in the discrete part of the spectrum (i.e., below the $1s$ ionization threshold) were assigned to electron promotion into Rydberg orbitals. This interpretation was in line with the view held at the time concerning similar features in valence-level excitation spectra (see discussion in Vol. 1 of Ref. [21]). Even in the latter area, however, the assignment of features below the ionization threshold had long been a subject of debate. For instance, Mulliken [22] was of the opinion that an assignment of a particular orbital in terms of "Rydberg" or "valence" represented only alternative descriptions of the same physical entity. An interpretation of the discrete part of the spectrum solely in terms of Rydberg orbitals must necessarily also assume that the antibonding valence orbitals appear as shape resonances in the ionization continuum.

More recent experimental work has made it clear that the exclusively "Rydberg" interpretation of core-level excitation spectra may not always apply [23]. In the simplest hydride HF the lowest F $1s$ excitation is clearly associated with the strongly antibonding σ^* orbital F $2p_z$-H $1s$) leading to direct dissociation of the excited mole-

cule. In the case of the other hydrides in this row the situation is certainly much less transparent. What one might reasonably expect, however, is an intermediate situation between that of HF and the other extreme where the $1s$-σ^* excitations appear above the K edge. That the lowest hydride K-electron excitations (in particular for water) are perhaps described best as σ^*-Rydberg mixtures has in fact already been suggested in previous experimental [24] and theoretical studies [25,26].

The σ^* vs. Rydberg problem in molecular K-shell spectra has recently been discussed by Ishii *et al.* [27]. These authors give a list of experimental criteria with which σ^* and Rydberg excitations can be distinguished. Simpler and less ambiguous access to the characterization of the excited states is provided in principle by the theoretical approaches. Here, however, the most obvious procedure, namely, the inspection of the respective orbitals as visualized by plotting the corresponding electron densities, is often not conclusive because the spatial extension of the σ^* orbitals and the lowest Rydberg orbitals is somewhat similar. It transpires that the variation of both the excitation energies and the oscillator strengths as a function of the X-H (X=C, N, O) bond length is more useful. Possible σ^* character should then reveal itself a distinct decrease of the excitation energy with increasing X-H distance and by a large variation of the oscillator strength. Pure Rydberg states, on the other hand, are expected to behave energetically similar to the ionic core state and their vertical electronic oscillator strengths should be largely independent of the X-H distance. In the present study we have used this approach to obtain more information on the K-shell excitations in H_2O, NH_3, and CH_4.

An outline of the paper is as follows. After briefly describing some experimental aspects in Sec. II, the polarization propagator approach is discussed in Sec. III. In Sec. IV we consider the experimental spectra and the results of calculations for the three molecules in the order H_2O, NH_3, and CH_4. It proves somewhat simpler to start with the water molecule because of its lower symmetry and the absence of vibrational structure, even though the experimental spectrum shows evidence for direct dissociation. In Sec. V we briefly discuss some general points arising from the preceding sections and summarize our main findings.

II. EXPERIMENT

The present data were recorded on the "Dragon" monochromator (beamline U4B) [11] at the National Synchrotron Light Source at Brookhaven National Laboratory. This monochromator is a cylindrical mirror, spherical grating design with a translating exit slit. A resolving power of $\sim 10^4$ has already been reported at the carbon K edge using an 800-line/mm grating; a carousel of three gratings with an interchange mechanism gives a similar resolving power and intensity at the nitrogen and oxygen K edges [15,17,18]. Monochromatized light passes through an absorption cell approximately 100 mm long. The transmitted light intensity is measured by secondary electron emission from a gold target. A gas phase sample of either H_2O, NH_3, or CH_4 is maintained at a pressure of approximately 1 Torr in the cell. A scan of the photon energy with sample present is followed by an identical scan with the absorption cell evacuated. Normalization with an empty cell spectrum is necessary to remove features due to absorption in the optical system. Due to long-term drift effects it is not possible to measure each spectrum on an absolute photon energy scale. The present spectra are referenced to EELS data and therefore have an accuracy of the order of ± 0.2 eV. However, due to the high precision of the grating drive mechanism and the relatively good short-term stability, the energy scale of each of the individually recorded spectra has a relative accuracy of the order of ± 10 meV.

III. THEORETICAL STUDIES

The direct calculation of (vertical electronic) excitation energies

$$e_m = E_m - E_0 \tag{1}$$

and dipole transition moments

$$T_m = \left\langle \Psi_m \left| \sum_{i=1}^{N} \underline{r}^{(i)} \right| \Psi_0 \right\rangle \tag{2}$$

was performed using a polarization propagator method referred to as the second-order algebraic diagrammatic construction [ADC(2)] [28]. Here $|\Psi_m\rangle$ and E_m denote the electronic states and energies, respectively, of the system under consideration, the ground state being labeled by $m=0$. The ADC(2) method has been applied previously to K-shell excitation in N_2, CO[20], and H_2CO [29]. For a full description of the computational details the reader is referred to Ref. [20]. In brief, the excitation energies e_m are obtained as the eigenvalues of a Hermitian secular matrix $(\underline{K}+\underline{C})$ according to

$$(\underline{K}+\underline{C})\underline{Y} = \underline{Y}\,\underline{E}, \quad \underline{Y}^{\dagger}\underline{Y} = \underline{1} \; . \tag{3}$$

Here $\underline{Y}$ denotes the matrix of eigenvectors and $\underline{E}$ is the diagonal matrix of the eigenvalues. The secular matrix $\underline{K}+\underline{C}$ is defined with respect to a configuration space comprising single and double excitations in the Hartree-Fock (HF) ground state; its first part $\underline{K}$ is a diagonal matrix containing zeroth-order HF excitation energies, while the matrix $\underline{C}$ referred to as the effective interaction matrix introduces perturbation expansions in the electronic Coulomb repulsion up to second order. In Refs. [20] and [28] explicit expressions have been given both for the matrix elements of $\underline{C}$ and for the so-called effective transition amplitudes $f_{J,pq}$. The latter quantities may be combined with the components of the mth eigenvector and the single-particle dipole integrals $\langle \varphi_p | \underline{r} | \varphi_q \rangle$ to yield the dipole transition moments of Eq. (2) according to

$$T_m = \sum_{J,p,q} Y^*_{Jm} f_{J,pq} \langle \varphi_p | \underline{r} | \varphi_q \rangle \; . \tag{4}$$

Here the summation extends over the excited electron configurations J and the single-particle states labeled by p and q, respectively. In the following, the dipole oscillator strength averaged over the molecular orientations

$$f_m = \tfrac{2}{3} e_m |T_m|^2 \tag{5}$$

(in atomic units) will be used as a measure of the spectral intensity.

As has been discussed in Ref. [28], the ADC(2) method allows a consistent treatment of single excitation energies and transition moments through second order in the electronic repulsion. This means that ground-state correlation and the effect of triple excitations in the excited states are taken into account (through second order), while the explicit ADC(2) configuration space comprises single and double excitations only. The present ADC treatment presupposes a Hartree-Fock calculation for the ground state of the molecule under consideration. Thus the effect of electronic relaxation, i.e., the adjustment of the valence orbitals to a core-level vacancy, is not taken into account from the outset, but has to be generated at the particular level of the ADC approximation. In spite of this drawback, fairly accurate results may be expected for the single excitations. The description of doubly excited states, on the other hand, will suffer from the incomplete consideration of relaxation.

The input data (orbital energies, dipole, and Coulomb integrals) for the ADC calculations described here were obtained from ground-state Hartree-Fock calculations. The self-consistent-field (SCF) basis sets used in these calculations for C, N, and O consisted of a Dunnings $9s/5p$ [30] set of Cartesian Gaussian functions augmented by a d-type polarization and s- and p-type diffuse functions. Contractions were employed only for the first four s and two p functions using the contraction coefficients of Ref. [30]. Further contractions influenced markedly the final excitation energies as was tested by comparison with calculations using the uncontracted SCF basis set. The exponents for the d functions were 0.6 (C), 0.98 (N), and 0.8 (O). Up to six and seven diffuse s and p functions, respectively, were introduced to reproduce the lowest $1s$-to-Rydberg transitions. Their exponents were chosen according to the recipe of Kaufmann, Baumeister, and Jungen [31]. For the hydrogen atoms Dunnings $3s$ contraction of $4s$ functions and a set of p-type polarization functions with the exponent $\alpha = 1.0$ were used. At the respective experimental ground-state equilibrium geometries [32] the following total HF energies were obtained: $-76.050\,39$ a.u. (H_2O), $-56.211\,31$ a.u. (NH_3), and $-40.205\,67$ a.u. (CH_4). In the ADC(2) secular equation configurations with zero and two $1s$ vacancies were disregarded. This approximation, referred to as the core-valence separation (CVS), is justified due to the large energy separation and small coupling matrix elements between the configurations with different $1s$ occupation numbers. As has been discussed in Ref. [20], the effect of the CVS approximation is a slight increase (about 0.4 eV) in the excitation energies. Using a spin-free formulation and exploiting spatial symmetry to the extent of the largest Abelian subgroup of the molecular point groups, secular matrices of dimension 3000–5000 had to be handled. An efficient block Davidson routine was employed to calculate the energetically lowest eigenvalues and the corresponding eigenvectors [33].

In order to obtain information on the vibrational structure of the $1s$ excitation bands as well as to throw some light on the Rydberg versus valence problem, calculations were also performed for symmetrically stretched and bent nuclear configurations. The corresponding variation of excitation energies was used to determine the vibrational coupling coefficients

$$k_i = \frac{1}{\sqrt{2}} \left[\frac{\partial E}{\partial Q_i} \right]_0 . \tag{6}$$

Here Q_i denote dimensionless totally symmetric normal coordinates associated with the electronic ground state; the subscript 0 indicates that the derivative has to be taken at the ground-state equilibrium geometry. To a good approximation, the Franck-Condon factor for a transition characterized by zero and m quanta of the mode ν_i in the initial and final state, respectively, may be calculated according to [34]

$$f_i(m,0) = \exp(-a_i) \frac{a_i^m}{m} , \tag{7a}$$

where the vibrational strength parameter a_i combines the coupling coefficient k_i and the frequency ω_i according to

$$a_i = \left[\frac{k_i}{\omega_i} \right]^2 . \tag{7b}$$

The second moment

$$\Delta_i = 2(2\ln 2)^{1/2} |k_i| \tag{8}$$

of the $f_i(m,0)$ progression may serve as a measure of the vibrational width associated with the excitation of the mode ν_i.

IV. RESULTS

A. Water

The oxygen K-shell absorption spectrum of H_2O, taken with a resolution of approximately 120 meV, is shown in Fig. 1. The energy positions and assignments of the

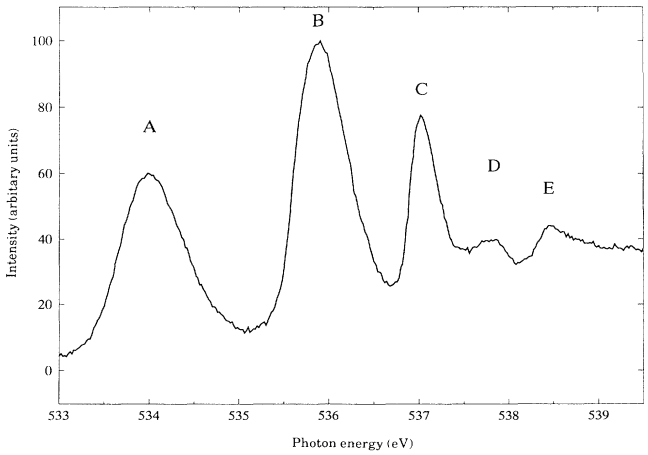

FIG. 1. The oxygen $1s$ photoabsorption spectrum of the water molecule in the region below the ionization threshold.

peaks labeled in the figure are given in Table I, together with the excitation energies and intensities calculated using the ADC(2) method. Overall the spectrum resembles the EELS spectrum reported by Wight and Brion [1]. It shows three strong peaks $A-C$ and two weaker peaks D and E below the ionization threshold. In spite of the higher resolution in the present experiment there is no evidence of vibrational fine structure in any of the features. A previous O 1s photo-absorption spectrum of H_2O taken at a much lower resolution has been reported by Akimov, Vinogradov, and Zimkina [9].

The ground-state electronic configuration of H_2O is

$$1a_1^2 2a_1^2 1b_2^2 3a_1^2 1b_1^2 (^1A_1) .$$

The outermost $1b_1$ orbital is largely nonbonding and mainly associated with the oxygen $2p_x$ atomic orbital. The in-plane components $2p_z$ and $2p_y$ of the oxygen $2p$ orbitals combine with the symmetric and antisymmetric linear combination of the H 1s orbitals, thereby forming the O—H bonding orbitals $3a_1$ and $1b_2$, respectively. As their counterparts we have to expect antibonding valence-type (σ^*) orbitals of a_1 and b_2 symmetry in the virtual spectrum. As will be discussed below, much of this σ^* valence character is contained in the first (O 1s-$4a_1$) and second (O 1s-$2b_2$) excited states, respectively. This has already been proposed by Diercksen *et al.* [25].

The ADC(2) results for the absolute excitation energies are somewhat lower than the experimental values. After increasing the theoretical values by a relativistic correction of 0.4 eV, the discrepancy is 0.8 eV for the O 1s-$4a_1$ excitation. The energy separations of the features $A-C$ and their relative intensities are well described by the present calculations. Previous theoretical studies of the K-shell excitations in H_2O using the ΔSCF method (i.e., separate HF calculations for the ground and excited states) have been reported by Ågren, Svensson, and Wahlgren [35] and by Deutsch and Curtiss [36]. In particular, the former calculations agree well with our results for the energies of the four lowest states. Intensities of O 1s excitations in H_2O have been calculated by Diercksen *et al.* [25] using the frozen-core Hartree-Fock (FCHF) method. Although the relative oscillator strengths for the first three transitions agree well with our results, the absolute FCHF values exceed those of the ADC(2) calculation by a factor of 4. This discrepancy is presumably due to the neglect of electronic relaxation in the FCHF method.

The present calculations also describe satisfactorily the O 1s-ns and O 1s-np Rydberg series up to $n=5$. Here the O 1s-np states are split into a_1, b_1, and b_2 components by the anisotropic molecular field. The admixture of a_1^* and b_2^* antibonding valence character in the lower members of the O 1s-$ns(a_1)$ and O 1s-$ns(b_2)$ series, respectively, is reflected by deviations from the usual quantum-defect (QD) representation and large $np(b_1)$-$np(b_2)$ energy splittings. The O 1s-$np(b_1)$ series, on the other hand, is unperturbed by valence admixtures and is well represented by the QD parametrization $E_n = I - R/(n-\delta_n)^2$ with $\delta_n \sim 0.7$ and $I = 538.15$ eV. Note that the value used here for I is about 1.8 eV below the experimental ionization potential of 539.9 eV [37]. The larger part (1.3 eV) of this discrepancy is associated with the shift of excita-

TABLE I. Excitation energies and relative intensities in the O 1s excitation spectrum of H_2O.

	Excitation energy (eV)			Rel. oscillator strength[b]	
Transition	ADC(2)		Expt.[a]	ADC(2)	FCHF[c]
O 1s-$4a_1/3s$	532.76	534.0	(A)	0.516	0.55
$2b_2/3p$	+1.95	+1.9(B)		1.000	1.00
$3p(b_1)$	2.83			0.245	0.243
		+3.0(C)			
$3p(a_1)$	2.94			0.155	0.119
$4s(a_1)$	3.32			0.117	0.016
$4p(b_2)$	3.77	+3.8(D)		0.369	0.029
$4p(b_1)$	4.16			0.080	0.001
$4p(a_1)$	4.20			0.054	0.001
$5s(a_1)$	4.32			0.044	0.004
		+4.4(E)			
$5p(b_2)$	4.45			0.150	0.008
$5p(b_1)$	4.67			0.037	7×10^{-4}
$5p(a_1)$	4.69			0.027	4×10^{-4}
$6s(a_1)$	4.74			0.024	0.003
$6p(b_2)$	4.80			0.072	0.003
$6p(b_1)$	4.99			0.037	
$6p(a_1)$	5.01			0.022	

[a]Results for peak maxima; energy calibration from Ref. [1].
[b]Absolute value for the O 1s-$2b_2$ transition is 0.0183 [ADC(2)] and 0.0725 (FCHF).
[c]Results of Ref. [35].

tion energies in the ADC(2) description.

Using ADC(2) the variation of the calculated excitation energies and oscillator strengths as a function of the symmetrical O—H bond stretching and bending has been studied. The results are shown in Table II. For the two lowest excitations, O $1s$-$4a_1/3s$ and O $1s$-$2b_2/3p$ one observes a considerable energy decrease with increasing O—H bond length. This behavior, which to a lesser extent is also seen for the higher $ns(a_1)$ and $np(b_2)$ transitions, provides a clear indication of the admixture of antibonding valence character in these states. By contrast, the O $1s$-$np(a_1)$ and O $1s$-$np(b_1)$ excitations show only little dependence on the O-H distance. As might be expected for the members of a Rydberg series, these energies behave very similarly to the O $1s$ ionization potential. The corresponding energy variations of the latter, calculated with the ΔSCF method (difference between the O $1s$ hole and ground-state HF energies), are shown in the last line of Table II for comparison. The different extent to which valence admixture occurs in the O $1s$ excitations is also reflected in the variation of the oscillator strength for different O-H distances. Here the large variations for the two lowest transitions O $1s$-$4a_1/3s$ and O $1s$-$2b_2/3p$ contrast with the almost constant oscillator strengths for the $np(a_1)$ and $np(b_1)$ manifolds.

The antibonding valence character of the O $1s$-$4a_1/3s$ and O$1s$-$2b_2/3p$ states raises the question as to whether these states are stable with respect to the dissociation process

$$H_2O^* \rightarrow OH^* + H \tag{9}$$

leading to an O $1s$ excited OH fragment and a H atom. A comparable dissociation process, resulting in the OH ($X\,^2P$) and H(^2S) fragments, is known for the valence $1b_1$-$4a_1$ excitation [21]. Here the potential-energy surface is repulsive for all H-O-H angles [38]. An indication of the dissociative nature of the O $1s$ excited states is the relatively large width (0.9 and 0.75 eV full width at half maximum FWHM, respectively) of the O $1s$-$4a_1$ and O $1s$-$2b_2$ peaks, as well as the absence of resolved vibrational structure. To obtain more information on the possibility of dissociation we have determined the exothermicity of the reaction (9) to be −3.3 eV (see Sec. V). The calculation confirms that hydrogen abstraction in the O $1s$ excited states is indeed energetically possible, but a more detailed investigation of the respective potential energy surfaces is necessary before the question of stability can be clarified.

Significant excitation of the ν_1 mode should accompany the O $1s$-$4a_1/3s$ and O $1s$-$2b_2/3p$ transitions if both states are not dissociative. The vibronic coupling constants listed in Table II show large values for k_1 (symmetrical stretching) and small values for k_2 (bending). In view of the high frequency (ν_1=475 meV) in the H_2O ground state [39] and an excitation strength a_1=0.5 [see Eq. (7)], the excitation of at least one quantum of the ν_1 mode should be clearly observable in the present experiment. Conversely, the absence of resolved vibrational structure must be interpreted as an indication that both the O $1s$-$4a_1/3s$ and O $1s$-$2b_2/3p$ transitions are dissociative. The coupling coefficients k_1 and k_2 in Table II may be used to estimate a vibrational width (which would also apply in the case of a repulsive potential surface)

$$\Delta = 2(2\ln 2)^{1/2}(k_1^2 + k_2^2)^{1/2} . \tag{10}$$

A value of Δ=0.8 eV results for both transitions in good agreement with the experimental widths, 0.9 and 0.75 eV, respectively.

TABLE II. Variation of the excitation energy (upper lines) and oscillator strength (lower lines) for the O $1s$ excitations in H_2O as a function of symmetrical stretching and bending. Right-hand side: vibrational coupling constants k_1 and k_2 for the totally symmetrical modes and the corresponding vibrational widths $\Delta=(\Delta_1^2+\Delta_2^2)^{1/2}$ [see Eq. (8)].

	Energy variations (eV) Oscillator strengths ($10^4 f$)				Vibrational coupling parameters (eV/bohr)		
State	$R_e-0.1$	R_e	$R_e+0.1$	$\alpha_e+10°$	k_1	k_2	Δ(eV)
O $1s$-$4a_1/3s$	+0.24	0	−0.31	−0.07	−0.337	−0.019	0.79
	70	95	123	82			
$2b_2/3p$	0.23	0	−0.31	−0.14	−0.332	−0.047	0.79
	136	183	239	170			
$3p(b_1)$	0.05	0	−0.05	−0.13	−0.063	−0.051	0.19
	46	45	44	45			
$3p(a_1)$	0.03	0	−0.5	−0.15	−0.051	−0.059	0.19
	29	28	27	28			
$4s(a_1)$	0.13	0	−0.14	−0.13	−0.167	−0.048	0.41
	17	21	26	21			
$4p(b_2)$	0.16	0	−0.20	−0.09	−0.222	−0.031	0.53
	69	68	69	60			
$4p(b_1)$	0.06	0	−0.07	−0.14	−0.082	−0.055	0.30
	15	15	15	15			
$4p(a_1)$	0.05	0	−0.07	−0.14	−0.076	−0.055	0.22
	10	10	10	9			
O $1s$ IP	0.04	0	−0.06	−0.16			

The third peak in the O 1s absorption spectrum (C) is distinctly narrower [0.4 eV FWHM] than the first and second peak. According to our calculations this peak has to be assigned to a superposition of transitions into two adjacent states (0.1-eV energy separation), namely the b_1 and a_1 components of the O 1s-3p Rydberg state. The small coupling parameters k_1 and k_2 (see Table V) indicate the absence of significant vibrational excitation in either of these transitions. This assignment, originally suggested by Wight and Brion [1], has been confirmed by the previous ΔSCF [35] and FCHF [25] calculations yielding, however, somewhat larger values of 0.3 and 0.2 eV, respectively, for the energy separation.

Above peak C the identification of calculated transitions in the experimental spectrum becomes difficult. There are two O 1s-4$s(a_1)$ and O 1s-4$p(b_2)$ transitions in a 1-eV energy interval above the excitations corresponding to C which are predicted to have considerable intensities (10% and 30%, respectively, relative to B). The energy of the latter transition correlates with the center of the weak feature D, suggesting its assignment as O 1s-4$p(b_2)$. The lack of any resolved vibrational structure in this feature might be due to several reasons including strong vibrational excitation of the ν_1 mode, overlapping with vibrational progressions of the neighboring O 1s-4$s(a_1)$ and dissociative broadening. Towards higher energy the density of states becomes larger while the intensity of individual transitions drops markedly. The spectral feature E at 4.4 eV above the O 1s-4a_1/3s transition cannot be assigned as a single transition, but is the result of a complicated superposition of many individual lines.

B. Ammonia

Figure 2 shows the N 1s excitation of NH_3 and the fully deuterated isotopomer ND_3. The NH_3 spectrum may be compared with previously reported spectra obtained by EELS [1,4] and x-ray absorption [9]. The present data show somewhat more detail than the EELS spectrum of Sodhi and Brion [4] taken with a spectral resolution of 360 meV; no vibrational fine structure could be resolved. The energy positions (peak maxima) of the five distinct spectral features are summarized in Table III along with the EELS results of Sodhi and Brion [4] for NH_3. The results of our ADC(2) calculations are given in Table IV. The absolute excitation energies lie about 0.8 eV below the experimental peak maxima after a relativistic correction of 0.2 eV is taken into account. For the relative energies of the lowest transitions, the calculations agree well with the experimental findings and confirm the assignments suggested in the previous experimental [4] and theoretical studies [40,36] using a relaxed-core Hartree-Fock treatment. There is also remarkably good agreement between our results and those of Schwartz [40] for the energies of the lowest four transitions.

The ground-state electronic configuration of NH_3 is

$$1a_1^2 2a_1^2 3a_1^2 1e^4 ({}^1A_1) .$$

The $2a_1$ orbital and the two degenerate $1e$ orbitals represent the three N-H bonding orbitals, while the $3a_1$ orbital is mainly p_z and nonbonding in character. As in the case of H_2O, the expected valence-type antibonding σ^* orbitals, which are of a_1 and e symmetry, do not manifest themselves as distinct excited states but rather mix with the lowest N 1s-$ns(a_1)$ and N 1s-$np(e)$ Rydberg states, as discussed by Schwarz [26]. This can be substantiated by inspecting the variation of excitation energies and oscillator strengths shown in Table V for several symmetrical N-H stretching and H-N-H bending geometries. First we note that the N 1s ionization potential (last line in Table V) increases by about 0.19 eV for a N-H elongation of 0.1 a.u. This behavior can be rationalized essentially as an electrostatic effect, namely, the increase of ionization energy due to the withdrawal of charge (antiscreening) from the central atom. A similar dependence on the N-H distance is seen for the N 1s-

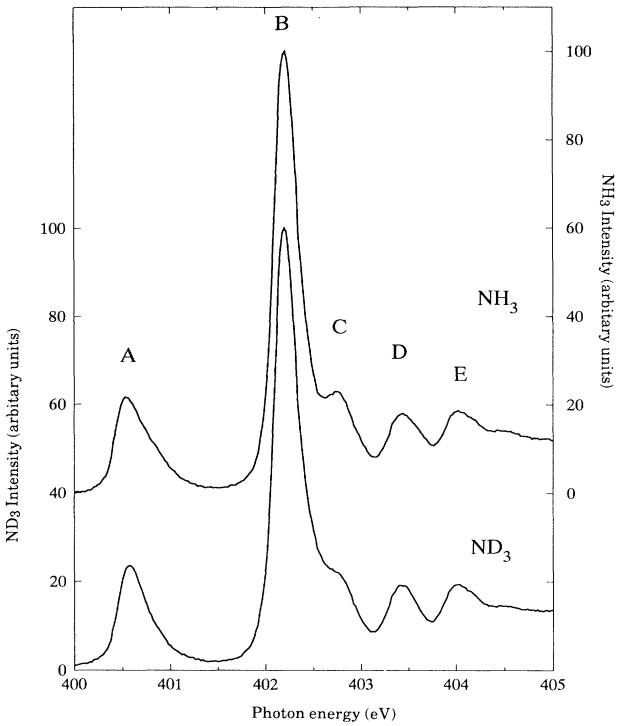

FIG. 2. The nitrogen 1s photoabsorption spectra of NH_3 and ND_3 in the region below the ionization threshold.

TABLE III. Energies of the N 1s excitations in NH_3 and ND_3 (eV).

Feature	assignment	NH_3 Present[a]	NH_3 EELS[b]	ND_3 Present[a]
A	N 1s-3$a(a_1)$	400.66	400.61	400.71
B	3$p(e)$	402.33	402.29	402.33
C	3$p(a_1)$	402.86	402.85	402.91
D	4$s(a_1)$	403.57	403.52	403.57
E	3$p(e)$	404.15	404.14	404.16

[a]The energy scale is calibrated with the N_2 N 1s-π^* ($\nu'=1$) transition at 401.10 eV.
[b]Sodhi and Brion (Ref. [4]).

TABLE IV. Calculated vertical energies and intensities of N 1*s* excitations in NH_3.

Transition	Excitation energy (eV) ADC(2)	Excitation energy (eV) Expt.		Rel. oscillator strength[a] ADC(2)
N 1*s*-3*s*(a_1)	399.78	400.8	(*A*)	0.20
3*p*(*e*)	+1.77	+1.7(*B*)		1.00
3*p*(a_1)	2.31	2.2(*C*)		0.16
4*s*(a_1)	2.88	2.9(*D*)		0.05
4*p*(*e*)	3.26	3.5(*E*)		0.56
4*p*(a_1)	3.49			0.05
5*s*(a_1)	3.68			0.02
5*p*(*e*)	3.82			0.40

[a]Absolute value for the N 1*s*-3*p*(*e*) transition is 0.024.

np(a_1) excitation energies establishing these states as pure N 1*s* to Rydberg excitations. Distinctly different, however, is the behavior of the lowest N 1*s*-*ns*(a_1) and N 1*s*-*np*(*e*) states. For the first excitation, N 1*s*-3*s*(a_1) there is almost no energy change connected with the variation of the N-H distance, which is also reflected by a very small vibrational coupling parameter k_1. This finding can be explained in terms of two mutually compensating effects: The energy required to remove an electron from the N 1*s* orbital (ionization potential) increases with the N-H distance. On the other hand, the population of an antibonding virtual orbital leads to decreasing excitation energy with N—H bond elongation. Thus the near constancy of the excitation energy indicates the presence of some valence-type σ^* character in the lowest excited state designated here in the Rydberg notation by N 1*s*-3*s*(a_1). For the higher members of the N 1*s*-*ns*(a_1) manifold the admixture of σ^* seems to be small and the transition energy behaves like the ionization potential.

Also for the first and second *e* states, N 1*s*-3*p*(*e*) and N 1*s*-4*p*(*e*), the energy variation pattern in Table V differs from that of the ionic case, though less pronounced than for the N 1*s*-3*s*(a_1) state. The $\sigma^*(e)$ valence character may therefore be distributed more uniformly over the lowest members of the N 1*s*-3*p*(*e*) manifold. A further indication for the presence of valence-type admixtures is the behavior of the oscillator strength as a function of the symmetrical N-H stretch coordinate. Substantial variations in its value are seen for the N 1*s*-3*s*(a_1) transition and for the first two members of the N 1*s*-*np*(*e*) series.

All transitions listed in Table V show considerable excitation of the H-N-H bending mode ν_2, the vibrational coupling parameter k_2 ranging from 0.070 to 0.230. The calculations predict an energy lowering (up to −0.40 eV) on going from a pyramidal to the planar configuration, indicating the possibility of a plane equilibrium geometry

TABLE V. Variation of the excitation energies (upper lines, eV) and vertical oscillator strengths (lower lines, $10^4 f$) for the N 1*s* excitations in NH_3 as a function of symmetrical stretching and bending. Right-hand side: vibrational coupling constants k_1 and k_2 for the totally symmetrical modes ν_1 and ν_2, respectively.

State	Energy variations (eV) oscillator strengths ($10^4 f$) $R_e-0.1$	R_e	$R_e+0.1$	$\alpha_{HNH}+10°$	Planar	Vibrational coupling constants (eV/bohr) k_1	k_2
N 1*s*-3*s*(a_1)	−0.07	0	+0.01	−0.10	−0.15	0.047	−0.067
	36	47	62	14	0		
3*p*(*e*)	−0.13	0	+0.07	−0.28	−0.39	0.117	−0.186
	182	238	323	208	198		
3*p*(a_1)	−0.19	0	+0.17	−0.33	−0.42	0.219	−0.230
	40	38	34	52	59		
4*s*(a_1)	−0.15	0	+0.11	−0.25	−0.35	0.158	−0.173
	9	12	16	4	0		
4*p*(*e*)	−0.12	0	+0.06	−0.25	−0.35	0.106	−0.167
	84	132	202	100	90		
4*p*(a_1)	−0.18	0	+0.15	−0.30	−0.42	0.201	−0.209
	13	12	11	17	19		
N 1*s* IP	−0.23	0	+0.19	−0.33	−0.45		

in the excited states. In the regime of the valence-electron excitations such a situation is known for the lowest excited singlet state $\bar{a}$ characterized as $1a''$-$3a'$ in D_{3h} symmetry [21]. Calculations by Ågren, Müller, and Nordgren [41] for the potential-energy surface of the N $1s$ hole state in the NH_3^+ cation predict a planar equilibrium configuration and, moreover, a distinctly lowered bending frequency ($\omega_2=54$ meV) with respect to the ground state ($\omega_2=140$ meV). An estimate of the bending mode frequencies in the N $1s$ excited states may be gained by comparing the energy variations in Table V with the ground-state double minimum potential along the ν_2 normal coordinate. For the N $1s$-$3s(a_1)$ transition this estimate gives $\omega_2=80$ meV. The shape of the corresponding spectral peak agrees with the assumption of a long progression of ν_2 excitations, the low frequency explaining the absence of resolved vibrational structure. The vibrational width $\Delta=200$ meV calculated according to Eq. (8) is somewhat smaller than the experimental finding. The N $1s$-$3s(a_1)$ peak in the ND_3 spectrum is distinctly narrower in accordance with the isotopic rule.

The second peak (B) in the N $1s$ absorption spectrum corresponds to a transition into the first excited state of e symmetry. The position of the peak maximum relative to the peak A agrees well with the calculated energy separation of the first two excited states. The vibrational structure of the N $1s$-$3p(e)$ transition may be rather complex due to the Jahn-Teller instability induced by the two degenerate vibrational e modes ν_3 and ν_4. A closer examination of the spectral profile has to be postponed until an adequate treatment for such a vibronic system is available. A study of this kind would also clarify whether the neighboring N $1s$-$3p(a_1)$ state has to be included in the vibronic calculation.

Although the absence of resolved vibrational structure in the present experiment may be explained solely by strong excitation of the ν_2 mode and by Jahn-Teller instability, one must also consider the possibility of dissociation as a broadening mechanism. In particular, the lowest excited state N $1s$-$3s(a_1)$ could be unstable with respect to hydrogen abstraction. The question of stability here is less obvious than in H_2O and can only be answered by an accurate calculation of the corresponding potential energy surfaces (see Sec. V).

Based on the transition energies alone, the three features C, D, and E correlate well with the subsequent three transitions N $1s$-$3p(a_1)$, $1s$-$4s(a_1)$ and $1s$-$4p(e)$. It should, however, be noted that the calculated vertical oscillator strengths, at least for the latter two transitions, do not agree with the experimental spectral weights. Obviously, substantial intensity modulations occur as a result of vibronic coupling and non-Franck-Condon behavior.

C. Methane

The present photoabsorption spectra of methane and methane d_4 in the carbon K-edge region are shown in Figs. 3 and 4 and reveal a wealth of spectral detail. The early synchrotron radiation absorption measurements [5,7,8] were taken at rather poor spectral resolution, dictated by the grazing-incidence monochromators then available. Higher resolution is seen in the EELS data of Wight and Brion [1] and Hitchcock, Pocock, and Brion [2], who assigned their spectra in terms of ns and np series of Rydberg levels approaching the C $1s$ ionization threshold. Our results agree well with the highest resolution EELS spectrum of Tronc *et al.* [3], but a significant improvement in signal-to-noise ratio and resolution is clearly evident. The energy positions of 22 spectral features in both the CH_4 and CD_4 spectra (Figs. 3 and 4) are listed in Table VI. The results of our ADC(2) calculations are presented in Table VII. The calculated (vertical) excitation energies are somewhat below the experi-

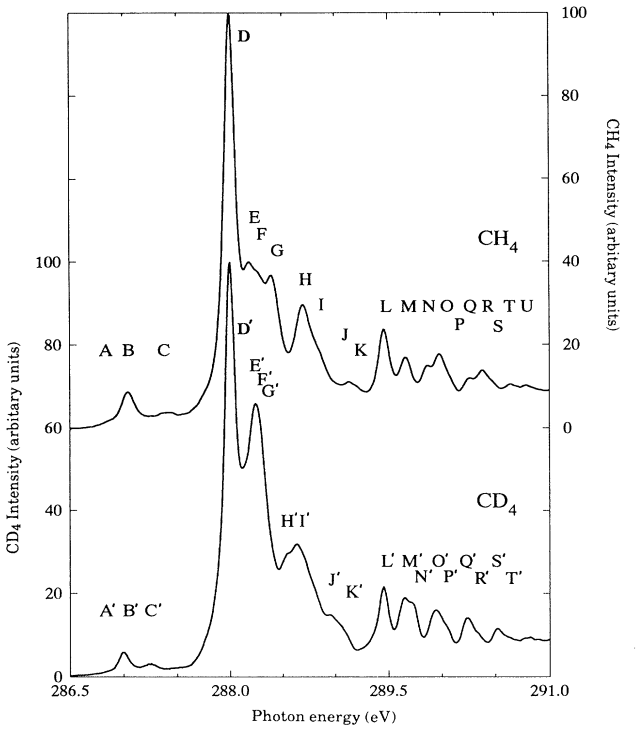

FIG. 3. The carbon $1s$ photoabsorption spectra of CH_4 and CD_4 in the region below the ionization threshold.

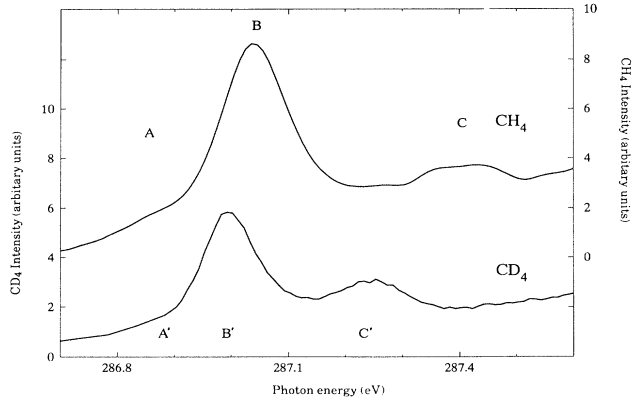

FIG. 4. The dipole-forbidden C $1s$-$4s(a_1)$ band in the carbon $1s$ photoabsorption spectra of CH_4 and CD_4.

mental peak maxima. The discrepancy, for example, in the energy of the C $1s$-$2t_2$ transition amounts to 0.3 eV, if a relativistic correction of 0.1 eV is taken into account. Accurate results slightly above the experimental energies have been obtained in previous theoretical studies using the ΔSCF method [6,36].

The ground-state electronic configuration of CH_4 is $1a_1^2 2a_1^2 1t_2^6 ({}^1A_1)$. The four C—H bonding orbitals are the $2a_1$ and the three degenerate $2t_2$ orbitals. The corresponding antibonding σ^* orbitals are also of a_1 and t_2 symmetry; as in the case of H_2O and NH_3, excitations into these orbitals are expected to mix with the Rydberg transitions. The weak feature B at approximately 287 eV in the spectrum has been assigned by Bagus, Krauss, and La Villa [6] as the dipole-forbidden C $1s$-$3s(a_1)$ Rydberg transition. Whereas the 0-0 vibrational band is strictly dipole forbidden, transitions to vibrational states of t_2 symmetry, e.g., 1_0^n-3_0^1 transitions, may be observed as a result of non-Franck-Condon behavior of the respective transition moment. The deviation from the Franck-Condon approximation may, for instance, be induced by vibronic coupling of the C $1s$-$3s(a_1)$ state with the neighboring C $1s$-$3p(t_2)$ state [2,6]. In methane, two modes, ν_3 and ν_4, of t_2 symmetry are found, with ground-state frequencies $\omega_3 = 374$ (280) meV and $\omega_4 = 162$ (123) meV, respectively, the values in parentheses referring to CD_4. A similar weak feature due to the dipole-forbidden $1s$-a_1 excitation is also found in the photoabsorption spectra of SiX_4 compounds (X = H,F,Cl, etc.) [42,43].

TABLE VI. Excitation energies and assignments for the C $1s$ photoabsorption spectra of methane and methane d_4.

	CH_4				CD_4
	Energy		Assignments		Energy
Peak	Present	Ref. [3]	Ref. [3]	Present	Peak	Present
A	286.86		-	$3s(a_1)+\nu_4$	*A'*	286.87
B	287.04	287.05	$3s$	$+\nu_3$	*B'*	286.99
C	287.41		-	$+\nu_1,\nu_3$	*C'*	287.24
D	288.00	288.00	$3p$		*D'*	288.00
E	288.19				*E'*	unresolved
F	288.27	288.24	$3p+\nu$		*F'*	unresolved
G	288.40	288.37	$3p+\nu$	$3p(t_2)$	*G'*	unresolved
H	288.69	288.70			*H'*	288.53
I	288.86				*I'*	288.63
					J'	288.95
J	289.13	289.14	$4s$		*K'*	289.05
				$4s(a_1)$		
K	289.21					
L	289.46	289.44	$4p$		*L'*	289.45
M	289.66	289.65	$4p+\nu$	$4p(t_2)$	*M'*	289.65
N	289.87	289.83	$5s$		*N'*	289.72
O	289.98	290.01	$5p$		*O'*	289.95
				$5p(t_2)$		
P	290.06				*P'*	290.04
Q	290.26				*Q'*	290.24
R	290.38			$6p(t_2)$	*R'*	290.34
S	290.48				*S'*	290.52
T	290.64				*T*	290.62
				$np(t_2)$		
U	290.78					
Z		290.76	$(1s)^{-1}$			

TABLE VII. Calculated vertical transition energies of the C $1s$ excitations in CH_4.

	Excitation energy (eV)	
Transition	ADC(2)	Experiment
C $1s$-$3s(a_1)$	−1.30	~−0.96 (*B*)
$3p(t_2)$	287.63	0 (*D*−*I*)
$4s(a_1)$	+0.95	~1.3 (*J*,*K*)
$4p(t_2)$	+1.33	~1.5 (*L*−*N*)
$5s(a_1)$	+1.68	
$5p(t_2)$	+1.78	~1.9 (*O*,*P*)
$6s(a_1)$	+2.04	
$6p(t_2)$	+1.92	~2.4 (*Q*−*S*)

The spectra shown in Fig. 4 were taken at an increased sample pressure and cover the region around 287 eV. In addition to the peak *B* (*B'*) at 287 eV one can clearly see a weaker shoulder *A* (*A'*) just below 286.9 eV and another feature *C* (*C'*) on the high-energy side. Assuming that the excited-state frequencies are similar to those in the ground state, the observed features fit reasonably well to the vibrational transitions 4_0^1 (*A*), 3_0^1 (*B*), and $1_0^1 3_0^1$ (*C*) for both CH_4 and CD_4 species. From the energy separation of the peaks *B* (*B'*) and *C* (*C'*) we obtain a value of 370 meV (250 meV) for the ν_1 frequency in the excited CH_4 (CD_4) state. According to the assignment given here, one would expect an isotope shift of about 90 meV for the peaks *B* and *B'* (arising from the distinct ν_3 frequencies). The experimental shift in Fig. 4, however, amounts to only 40 meV, which may partly be a result of the alignment of the two spectra as described above. The isotope effect on the intensity of the 3_0^1 peak *B* has been examined by Hitchcock, Pocock, and Brion [2]. In contrast to a prediction of Bagus, Kraus, and LaVilla [6], an ~20% decrease of intensity was found when going from CH_4 to the fully deuterated species. Our experiment shows a decrease of about 35%, the small discrepancy being perhaps due to an electric quadrupole contribution in the EELS data of Hitchcock, Pocock, and Brion [2].

A complex spectral profile between 287.6 and approximately 289.0 eV, comprising the features *D*−*I* in Fig. 3, is associated with the C $1s$-$3p(t_2)$ transition. The threefold degeneracy of the electronic state and the presence of two t_2 modes (ν_3,ν_4) constitute a complicated Jahn-Teller system which will lead to a large manifold of vibronic final states. Accordingly, we have to expect that the observed spectral curve is the result of complicated superposition of many densely lying individual lines. The very clear differences between the CH_4 and CD_4 spectra directly indicate the importance of vibronic effects. A re-

liable analysis of the vibrational structure would have to be based on dynamical calculations that account adequately for the coupling between the electronic and nuclear motion. Since a study of this kind is still lacking, we refrain from assigning any of the individual peaks ($D-I$), which was attempted by Tronc *et al.* [3] and by Robin [21].

About 1 eV above the C $1s$-$3p(t_2)$ energy our calculation predicts the next transition characterized as C $1s$-$4s(a_1)$. Similar to the first member of the $ns(a_1)$ Rydberg series, vibrational states with one quantum in the ν_3 or ν_4 mode may obtain intensity due to non-FC behavior. It seems likely that the small features (J and K) in the CH_4 spectrum can be associated with the C ($1s$-$4s(a_1)$ transition. Towards higher energy, as the energy separation of states becomes smaller, we must expect that in addition to the Jahn-Teller instability of the C $1s$-$np(t_2)$ states nonadiabatic effects arise from vibronic coupling between neighboring states both of a_1 and t_2 symmetry. Thus a detailed explanation of the spectral profile including the individual features $L-U$ also cannot be given at the present stage. Nevertheless, we may attempt to correlate some of the calculated transitions with selected groups of spectral features. A quite natural choice adopted in Tables VI and VII is to distinguish three groups ($L-N$), (O,P), and ($Q-S$) in the CH_4 spectrum. The tentative assignment as C $1s$-$np(t_2)$ transitions with $n=4-6$ seems to be justified by the calculated energy separations, except perhaps for $n=6$, where the experimental energy is somewhat too large.

Table VIII shows the variation of the C $1s$ excitation energies as a function of the C—H bond length. For comparison the C $1s$ ionization energy changes (calculated on the ΔSCF level) are also given here. The antiscreening effect for the C $1s$ potential connected with the withdrawal of the surrounding H atoms is considerably more effective than for NH_3, resulting in an increase of the ionization energy by about 0.4 eV per 0.1 a.u. C—H bond elongation. The C $1s$-$ns(a_1)$ manifold of states shows almost perfect ionic behavior; there is no indication of possible $\sigma^*(a_1)$ valence admixtures, at least for the lowest members $n=3-5$ considered in Table VIII.

TABLE VIII. Variation of C $1s$ excitation energies (upper lines, eV) and oscillator strengths (lower lines, $10^4 f$) in CH_4 as a function of the C-H distance R (a.u.).

State	$R_e-0.1$	R_e	$R_e+0.1$	$R_e+0.2$
C $1s$-$3s(a_1)$	−0.38	0	+0.31	+0.55
$4s(a_1)$	−0.41	0	+0.37	+0.69
$5s(a_1)$	−0.42	0	+0.38	+0.72
C $1s$-$3p(t_2)$	−0.42	0	+0.39	+0.71
	192	233	302	420
$4p(t_2)$	−0.41	0	+0.33	+0.49
	84	108	376	588
$5p(t_2)$	−0.36	0	+0.18	+0.43
	68	359	272	42
$6p(t_2)$	−0.23	0	+0.36	+0.71
	320	108	1	0
C $1s$ IP	−0.47	0	+0.44	+0.85

For the C $1s$-$np(t_2)$ transitions Table VIII also contains the vertical oscillator strengths for selected C-H distances. A close examination of both the energy and intensity variations of the manifold of t_2 states reveals the presence of an antibonding valence-type state that diabatically crosses the C $1s$-$np(t_2)$ Rydberg states $n=6,5,4$, and 3 in the region $R_e-0.1$ to $R_e+0.2$ a.u. This can be seen by the sudden jumps in the oscillator strength: for $n=6$ at R_e, for $n=5$ at R_e (increase) and at $R_e+0.2$ a.u. (decrease), for $n=4$ at $R_e+0.1$ a.u., and for $n=3$ at $R_e+0.2$ a.u. The "perturbing" virtual valence level also causes noticeable deviations of the otherwise ionlike behavior of the excitation energies, e.g., for $n=6$ at $R_e-0.1$ a.u., for $n=5$ at $R_e+0.1$, for $n=5$ and 4 at $R_e+0.2$ a.u. The perturbing level obviously has to be associated with the $\sigma^*(t_2)$ orbital and will certainly play a role in the dynamics of the C $1s$ transitions at higher energy.

V. GENERAL DISCUSSION AND CONCLUSIONS

In spite of the high experimental resolution of the present K-shell photoabsorption spectra, distinct vibrational structure could only be resolved and assigned in the case of the dipole-forbidden C $1s$-$3s(a_1)$ transition in CH_4 and CD_4. An obvious explanation for the broadening of the spectral features—apart from experimental resolution and lifetime effects—is the dissociation of the excited species. Indeed, one might reasonably expect that all three hydride molecules will eject a hydrogen atom upon excitation of a K-shell electron. This is suggested by the $Z+1$ model (see Schwarz [44]) relating the core-excited molecules OH_2^*, NH_3^*, and CH_4^* to the systems FH_2, OH_3 and NH_4 in corresponding states. From a chemical point of view, none of these systems is expected to be stable with respect to hydrogen abstraction. The ionic X $1s$ single-hole species, on the other hand, corresponding to the FH_2^+, OH_3^+, and NH_4^+ cation ground states in the $Z+1$ model, are well equipped to bind all their hydrogens, and the addition of a Rydberg electron will not substantially affect this stability. Indeed, bound states of the neutral radicals FH_2, OH_3, and NH_4, referred to as Rydberg molecules, are known to exist from numerous experimental and theoretical studies (see, e.g., Raynor and Herschbach [45] and Kaspar, Smith, and McMaster [46]). By analogy we may conclude that those K-shell excitations described as X $1s$ Rydberg transitions are stable, or at least metastable, with respect to fragmentation. By contrast, transitions to states with sufficiently large X $1s$-σ^* admixtures are thought to lead to direct dissociation. In order to clarify whether dissociation is actually effective in a particular transition, the appropriate potential-energy surface has to be examined. Examples of dissociative broadening are presumably the O $1s$-$4a_1/3s$ and O $1s$-$2b_2/3p$ transitions (peaks A and B in Fig. 1) in H_2O. Here the large coupling parameter k_1 and frequency ω_1 for the symmetrical O-H stretching mode are not compatible with the observed spectral profile, unless a dissociative behavior is assumed.

From a thermodynamic cycle involving the O—H bond energy (5.44 eV [47]) in the H_2O ground state, the electron affinity of OH (1.83 eV [48]), and the O 1*s* ionization energy of OH^- (525.8 eV [49]) we have estimated the exothermicity ΔE of the fragmentation reaction $OH_2^* \rightarrow OH^* + H$ for the lowest O 1*s* excitation. The resulting value $\Delta E = -3.3$ eV shows clearly that the fragmentation is energetically feasible. The instability of the OH_2 species is furthermore corroborated by the fact that no stable FH_2 ground state has been found. We note that Coulman *et al.* [50] have observed fragmentation of the water molecule in adsorbed monolayers and in the condensed phase at the O *K* edge to give H^+ ions. A sharp feature at ~534 eV in the H^+ yield from the monolayer appears to correspond to peak *A* in the gas-phase photoabsorption spectrum and has been assigned by the authors to the O $1s$-$4a_1$ transition. There is no simple 1:1 correspondence between the H^+ yield spectrum and the absorption spectrum at higher energies. Since it is extremely difficult in the photodesorption experiment to measure the neutral H atom yield, the relative importance of the two fragmentation channels is at present unknown.

For NH_3, the question as to whether the lowest excited state is dissociative is less clear, since another source of broadening comes into play, namely, the unresolved bending mode (ν_2) excitation. This more complex situation is also reflected by the $Z+1$ model, where the stability of the OH_3 ground state is still a matter of debate. Here the quality of the theoretical predictions depends quite sensitively on the accuracy of the computational schemes involved [51]. By contrast, the lowest excitation in CH_4, C $1s$-$4s(a_1)$, which is of pure Rydberg character, is obviously stable with respect to fragmentation, allowing the individual vibrational levels to be detected. This is also suggested by the $Z+1$ analogy: the NH_4 radical, discovered experimentally by Herzberg [52] in 1981, shows a substantial barrier along the ground-state dissociation path [46]. For transitions to final states of *e* and t_2 symmetry in NH_3 and CH_4, respectively, the Jahn-Teller coupling of electronic and nuclear motion will give rise to a dense manifold of final vibronic levels preventing the resolution of further spectral details.

To clarify the question of Rydberg versus valence (σ^*) character of the excited states we have examined the behavior of the excitation energies as a function of the distance R_{XH} between the central (X=C,N,O) and the H atoms. Pure Rydberg excitations should behave in a similar way as the X 1*s* ionization potential (IP), while antibonding valence character should lead to strong deviations from the IP behavior. A common trend, being smallest for H_2O and largest for CH_4, could be seen in the variation of the IP with R_{XH}: the increase of R_{XH} leads to a withdrawal of negative charge from the central atoms, which in turn causes a lowering of the electrostatic potential felt by an X 1*s* electron. This (anti-) screening effect is particularly pronounced on the zeroth-order level (Koopman's theorem) where the IP is given by the negative ground-state HF orbital energy $-\varepsilon_{X1s}$. For an increase $\Delta R_{XH}=0.1$ a.u. we have found the values $-\Delta\varepsilon_{X1s}=0.25$ eV (H_2O), 0.50 eV (NH_3), and 0.70 eV (CH_4). This is to be compared with the relaxed ΔSCF results $\Delta IP=-0.06$ eV (H_2O), 0.19 eV (NH_3) and 0.44 eV (CH_4). Obviously, relaxation reduces the static (anti-)screening effect, leading in the case of H_2O even to a slight decrease in the IP.

Besides the energy we have also considered the dependence of the (vertical) oscillator strength on R_{XH} which is expected to be strong for a final state with valence σ^* character. The conclusions drawn from the dynamical observations can be summarized as follows: For H_2O, most of the expected σ^* character is mixed in the first and second excitations, O $1s$-$4a_1/3s$ and O $1s$-$4b_2/3p$, which explains the dissociative nature of the corresponding energy surfaces. Similarly, in NH_3 the lowest excited state, N $1s$-$3s(a_1)$, is characterized by a strong $\sigma^*(a_1)$ admixture and the energy surface is probably dissociative here as well. Antibonding $\sigma^*(e)$ character is also present in the *e* manifold, but seems to be more uniformly distributed over several states. A different situation was found for CH_4. Here pure Rydberg character is found in the manifold of C $1s$-$ns(a_1)$ excitations, while in the t_2 manifold the presence of a C $1s$-$\sigma^*(t_2)$ excitation could be identified by distinct perturbations in both the vertical transition moments (oscillator strengths) and excitation energies of the C $1s$-$np(t_2)$ Rydberg series. With respect to the occurrence of shape resonances in the *K* electron continua it follows that in both H_2O and NH_3 only little σ^* character can be expected to appear above threshold. The same conclusion applies to the $\sigma^*(t_2)$ orbital in CH_4. The only case where according to our considerations a shape resonance associated with an *X*-H antibonding orbital may be expected is the a_1 continuum in CH_4. The *K* level photoabsorption above threshold does show a pronounced feature at 303 eV [1], but the other two hydrides also show weak features in a similar energy range. In this connection, the possibility of double excitations of the type X $1s$-σ^*, σ-σ^* cannot be discounted.

ACKNOWLEDGMENTS

J. S. acknowledges stimulating discussions with H. Köppel and D. Nordfors. We thank the Federal German Ministry of Research and Technology for financial support under Grant Nos. 05 490 FXB and 05 5VHF AB. The experimental work was carried out at the National Synchrotron Light Source, which is supported by the U.S. Department of Energy under Contract No. DE-AC02-76CH00016.

*Permanent address: Laboratory of Quantum Chemistry, Irkutsk University, Irkutsk 664003, Russia.

[1] G. R. Wight and C. E. Brion, J. Electron Spectros. **4**, 25 (1974).

[2] A. P. Hitchcock, M. Pocock, and C. E. Brion, Chem. Phys. Lett. **49**, 125 (1977).

[3] M. Tronc, G. C. King, R. C. Bradford, and F. H. Read, J. Phys. B **9**, L555 (1976); M. Tronc, G. C. King, and F. H.

Read, *ibid.* **12**, 137 (1979).
[4] R. N. S. Sodhi and C. E. Brion, J. Electron Spectrosc. Relat. Phenom. **36**, 187 (1985).
[5] H. W. Chun, Phys. Lett. **30A**, 445 (1969).
[6] P. S. Bagus, M. Krauss, and R. E. LaVilla, Chem. Phys. Lett. **23**, 13 (1973).
[7] W. Eberhardt, R.-P. Haelbich, M. Iwan, E. E. Koch, and C. Kunz, Chem. Phys. Lett. **40**, 180 (1976).
[8] F. C. Brown, R. Z. Bachrach, and A. Bianconi, Chem. Phys. Lett. **54**, 425 (1978).
[9] V. N. Akimov, A. S. Vinogradov, and T. M. Zimkina, Opt. Spektrosk. **53**, 476 (1982) [Opt. Spectrosc. (USSR) **53**, 280 (1982)].
[10] H. Petersen, Opt. Commun. **40**, 402 (1982); M. Domke, I. Mandel, A. Puschmann, C. Xue, D. A. Shirley, G. Kaindl, H. Petersen, and P. Kuske, Rev. Sci. Instrum. **63**, 80 (1992).
[11] C. T. Chen. Nucl. Instr. Methods A **256**, 595 (1987); C. T. Chen and F. Sette, Rev. Sci. Instrum. **60**, 1616 (1989).
[12] P. A. Heimann, F. Senf, W. McKinney, M. Howells, R. D. van Zee, L. J. Medhurst, T. Lauritzen, J. Chin, J. Meneghetti, W. Gath, H. Hogrefe, and D. A. Shirley, Phys. Scr. **T31**, 127 (1990).
[13] H. Maezaura, A. Toyoshima, Y. Kagoshima, K. Mari, and T. Ishikawa, Rev. Sci. Instrum. **60**, 1889 (1989).
[14] W. Eberhardt, K. J. Randall, J. Feldhaus, A. M. Bradshaw, R. F. Garrett, and M. L. Knotek, Phys. Scr. **41**, 745 (1990); K. J. Randall, J. Feldhaus, W. Erlebach, A. M. Bradshaw, E. Eberhardt, Z. Xu, Y. Ma, and P. D. Johnson, Rev. Sci. Instrum. **63**, 1367 (1992).
[15] C. T. Chen, Y. Ma, and F. Sette, Phys. Rev. A **40**, 6737 (1989).
[16] M. Domke, C. Xue, A. Puschmann, T. Mandel, E. Hudson, D. A. Shirley, and G. Kaindl, Chem. Phys. Lett. **173**, 122 (1990).
[17] Y. Ma, C. T. Chen, G. Meigs, K. Randall, and F. Sette, Phys. Rev. A **44**, 1848 (1991).
[18] F. X. Gadea, H. Köppel, J. Schirmer, L. S. Cederbaum, K. J. Randall, A. M. Bradshaw, Y. Ma, F. Sette, and C. T. Chen, Phys. Rev. Lett. **66**, 883 (1991).
[19] N. Kosugi, E. Shigemasa, and A. Yagishita, Chem. Phys. Lett. **190**, 481 (1992).
[20] A. Barth and J. Schirmer, J. Phys. B **18**, 867 (1985).
[21] M. B. Robin, *Higher Excited States of Polyatomic Molecules* (Academic, New York, 1974–1985), Vols. I–III.
[22] R. S. Mulliken, J. Am. Chem. Soc. **86**, 3183 (1964).
[23] A. P. Hitchcock and C. E. Brion, J. Phys. B **14**, 4399 (1981).
[24] H.-T. Wang, W. S. Felps, and S. P. McGlynn, J. Chem. Phys. **67**, 2614 (1977).
[25] G. H. F. Diercksen, W. P. Kraemer, T. N. Rescigno, C. F. Bender, B. V. McKoy, S. R. Langhoff, and P. W. Langhoff, J. Chem. Phys. **76**, 1043 (1982).
[26] W. H. E. Schwarz, Chem. Phys. **11**, 217 (1975).
[27] I. Ishii, R. McLaren, A. P. Hitchcock, and M. B. Robin, J. Chem. Phys. **87**, 4344 (1987).
[28] J. Schirmer, Phys. Rev. A **26**, 2395 (1982).
[29] J. Schirmer, A. Barth, and F. Tarantelli, Chem. Phys. **122**, 9 (1988).
[30] T. H. Dunning, J. Chem. Phys. **53**, 2823 (1970).
[31] K. Kaufmann, W. Baumeister, and M. Jungen, J. Phys. B **22**, 2223 (1989).
[32] Landolt-Börnstein, *Numercial Data and Functional Relationships in Science and Technology,* edited by K. H. Hellwege and A. M. Hellwege, New Series, Group II, Vol. 7 (Springer, Heidelberg, 1976).
[33] The computer-program package was written by F. Tarantelli, University of Perugia, Italy (1988).
[34] See, for example, L. S. Cederbaum and W. Domcke, Adv. Chem. Phys. **36**, 205 (1977).
[35] H. Ågren, S. Svensson, and U. I. Wahlgren, Chem. Phys. Lett. **35**, 336 (1975).
[36] P. W. Deutsch and L. A. Curtiss, Chem. Phys. Lett. **39**, 588 (1976).
[37] W. L. Jolly, K. D. Bomben, and C. J. Eyermann, At. Data Nucl. Data Tables **31**, (3), 433 (1984).
[38] G. Theodorakopoulos, I. D. Petsalakis, and R. J. Buenker, Chem. Phys. **96**, 217 (1985).
[39] Experimentally derived force constants have been used from A. R. Hoy, I. M. Mills, and G. Strey, Mol. Phys. **24**, 1265 (1972); A. R. Roy and P. R. Bunker, J. Mol. Spectrosc. **74**, 1 (1979).
[40] M. E. Schwartz, Chem. Phys. Lett. **40**, 1 (1976).
[41] H. Ågren, J. Müller, and J. Nordgren, J. Chem. Phys. **72**, 4078 (1980).
[42] S. Bodeur, I. Nenner, and P. Millié, Phys. Rev. A **34**, 2986 (1986).
[43] S. Bodeur, P. Millié, E. Lizon à Lugrin, I. Nenner, A. Fillipone, F. Boscherini, and S. Mobilio, Phys. Rev. A **39**, 5075 (1989).
[44] W. H. E. Schwarz, Angew. Chemie Int. Ed. **13**, 454 (1974).
[45] S. Raynor and D. Herschbach, J. Phys. Chem. **86**, 3592 (1982).
[46] J. Kaspar, V. H. Smith, and B. N. McMaster, Chem. Phys. **96**, 81 (1985).
[47] W. P. Kraemer, B. O. Roos, and P. E. M. Siegbahn, Chem. Phys. **69**, 305 (1982).
[48] P. A. Schulz, R. D. Mead, P. L. Jones and W. C. Lineberger, J. Chem. Phys. **77**, 1153 (1982).
[49] This value was calculated using the ADC(4) propagator method as described in G. Angonoa, O. Walter, and J. Schirmer, J. Chem. Phys. **87**, 6789 (1987).
[50] D. Coulman, A. Puschmann, W. Wurth, H.-P. Steinrück, and D. Menzel, Chem. Phys. Lett. **148**, 371 (1988); J. Chem. Phys. **93**, 58 (1990).
[51] G. I. Gellene and R. F. Porter, J. Chem. Phys. **81**, 5570 (1984).
[52] G. Herzberg, Faraday Discuss. Chem. Soc. **71**, 165 (1981).